Influence of sliding interfaces on the response of a layered viscoelastic medium under a moving load

Olivier Chupin, Armelle Chabot, Jean-Michel Piau, Denis Duhamel

Influence of sliding interfaces on the response of a layered viscoelastic medium under a moving load

O. Chupin [a,*], A. Chabot [a], J.-M. Piau [a], D. Duhamel [b]

[a] Université Nantes-Angers-Le Mans, Laboratoire Central des Ponts et Chaussées (LCPC), Route de Bouaye, BP 4129, 44341 Bouguenais Cedex, France
[b] Université Paris-Est, UR Navier, Ecole Nationale des Ponts et Chaussées, 6 et 8 Avenue Blaise Pascal, Cité Descartes, Champs sur Marne, 77455 Marne la Vallée, Cedex 2, France

This article presents a method to compute the response of a viscoelastic layered half-space to a moving load when interlayer slip is considered. The Navier equations of equilibrium are solved for each layer in the frequency domain. The solution in the spatial coordinate system is subsequently obtained by means of Fast Fourier Transform and quadrature rules applied to integrable singularities. Following the global solution technique, the developed method compiles all the interface and the boundary conditions within a global matrix and it solves a unique linear system per couple of wave numbers. This method proves to be effective and is validated in an elastic case by comparison with the ALIZE-LCPC software that implements the Burmister axisymmetric solution. The influence of the interface sliding condition on the response of a layered viscoelastic medium is studied through an application to pavement structures. In this application, the effect of the load speed on vertical and horizontal profiles of the longitudinal strain and the normal stress is analyzed. It is shown, inter alia, that the maximum extension in the medium is not systematically observed at the location of an interface and that, as expected, low speeds and interlayer slip are more damaging to the structure when either a strain or a stress criterion is considered.

Keywords:
Spectral methods
Moving load problem
Layered viscoelastic medium
Interface condition
Pavement engineering

1. Introduction

The theoretical response of a half-space under a moving load with static and dynamic components has been largely investigated in the past. The numerous applications that can be modeled within the frame of wave propagation have driven such efforts. Among all these applications one can refer to seismic problems, road and high speed railways engineering. As a consequence, studies in this area have considered many types of medium and loading, such as moving point loads or uniformly distributed normal and shear loads.

Early works by Sneddon (1952) or Cole and Huth (1958) have focused on two-dimensional problems and have used integral transform methods. Considering similar methods, Eason (1965) analyzed the three-dimensional response of a semi-infinite homogeneous and isotropic elastic solid under a point, a disk or a rectangular load moving at a uniform velocity. For application to cement concrete roads, railway tracks or bridges, several authors like Frýba (1972, 1987), Olsson (1991) or Sun (2006) preferred to model the pavement system as an elastic beam or plate resting on an elastic (Winkler) foundation excited by a moving force. Barros and Luco (1994), among others, extended prior works to the analysis of a three-dimensional multilayered half-space. They derived the steady-state displacements and stresses within a multilayered viscoelastic medium generated by a buried or a surface point load moving at constant speed. They used an approach based on an integral representation of the complete response in terms of wavenumbers, introducing layering effects by an exact factorization of the displacement in terms of generalized transmission and reflection coefficients. The Fourier transform is used in Barros and Luco (1994) to compute the response in the frequency domain prior to performing a Fast Fourier Transform (FFT) that leads to the solution in the spatial domain. Barros and Luco (1995) later deepened their analysis by introducing moving line load to the problem whose solution relied on a similar procedure to obtain Green's functions for a layered half-space. This approach had been used formerly by Luco and Aspel (1983a,b). About the influence of loading on the mechanical response, Hung and Yang (2000) gave insights into the mechanism of wave propagation for a viscoelastic half-space under moving loads of different types including dynamic components. In the pavement field, specific models have been developed to propose a more realistic representation of the complex contact problem of a tire on a pavement structure. These models handle non-uniform stresses that depend on the load speed and they account for the viscoelastic behavior of asphalt concrete layers.

Aside from semi-analytical methods, the solution of such three-dimensional problems has also been addressed by means of the boundary element method (Andersen and Nielsen, 2003) or the finite element method (Elseifi et al., 2006; Heck et al.,

* Corresponding author. Tel.: +33 240 845 786; fax: +33 240 845 994.
E-mail addresses: olivier.chupin@lcpc.fr (O. Chupin), armelle.chabot@lcpc.fr (A. Chabot), jean-michel.piau@lcpc.fr (J.-M. Piau), duhamel@lami.enpc.fr (D. Duhamel).

1998; Hornych et al., 2002). See also Hornych et al. (2007) for the treatment of problems involving non-linear behavior of soil layers. Nevertheless, semi-analytical methods are still developed in order to offer alternative tools to purely numerical methods. These tools are used for the design of engineering structures such as pavements. In this framework, several models compute semi-analytical solutions that do account for inertia forces (3D-Move (Siddharthan et al., 1998; Siddharthan et al., 2000) and ViscoRoute (Duhamel et al., 2005)) or do not (VEROAD (Hopman, 1996)). Otherwise from 3D-Move, the model implemented in ViscoRoute directly integrates the viscoelastic behavior of asphalt materials through the Huet–Sayegh model (Huet, 1963; Huet, 1999; Sayegh, 1965) which is particularly well-suited for the modeling of asphalt overlays (Chailleux et al., 2006; Nilsson et al., 2002). The models implemented in these tools consider a multilayered medium in which the layers can have a viscoelastic or an elastic behavior. Furthermore, they only assume full bonded conditions at the interface between layers. In spite of that, interface sliding is also encountered in real pavements as, for instance, in composite pavements in which the initial bonding between layers may eventually fail due the action of traffic (SETRA-LCPC, 1997). Generally, as far as multilayered structures are considered, free edges or vertical cracks across layers may produce debonding at interlayer locations, asking for specific modeling (Caron et al., 2006; Chabot et al., 2005). Consequently, it is necessary to evaluate the influence of the interlayer sliding condition on the global response of such structures if one wants to predict their long-term behavior.

So, the present article aims at developing a method to compute the mechanical response of a multilayered half-space with interlayer slip when excited by moving loads. Layers of the studied medium have either an elastic or a thermoviscoelastic behavior; the governing equations are exposed in Section 2. The solving procedure derived in Section 3 relies upon Fourier transformations and it computes the analytical solution in the frequency domain prior to calculating the spatial solution by means of FFT and quadrature rules. The solution in the wavenumber domain is obtained using matrix techniques which have already been used in many applications related to fields such as seismology or acoustic. In the review on the matrix techniques presented by Lowe (1995), two different approaches, with possible variants, are distinguishable. These are the transfer matrix method (Thomson–Haskell) and the global matrix method. The transfer matrix method (or "propagator matrix" method) was first developed by Thomson (1950) and Haskell (1953) for seismological applications. It consists in propagating the boundary conditions from one boundary of the system to the other through matrix multiplications. This method is known to encounter stability issues for high frequencies and large layer thicknesses. On the other hand, the global matrix method, which is used herein, was originally proposed by Knopoff (1964). It was first implemented by Randall (1967) and employed by number of researchers (for a quite comprehensive list, see Lowe, 1995) among which Schmidt and Jensen (1985) or Schmidt and Tango (1986) contributed to significant developments, in particular in terms of numerical efficiency and stability. The global matrix method consists in assembling a single matrix that gathers all the boundary relations. Then, the response solution for the vector of wave amplitudes may be readily obtained by inversion of the system matrix. According to Schmidt and Tango (1986), the global matrix approach yields both improved efficiency and versatility. The global matrix method has been implemented in several numerical programs. In particular, it is the basis of the early computer code SAFARI (Schmidt, 1987). Note that an upgraded version of SAFARI (named OASES) which provides higher numerical stability, was also developed at the Massachusetts Institute of Technology (Schmidt, 1999). So, contrary to Barros and Luco (1994) or Duhamel et al. (2005), the solving procedure presented in this article considers a global matrix instead of a recursive scheme involving transmission and reflection coefficients. In order to implement this method, we modified and extended the original ViscoRoute kernel (Duhamel et al., 2005). In Section 4, the implemented method is validated in elasticity by comparison with software ALIZE-LCPC (Autret et al., 1982). Afterwards, qualitative and quantitative results about the influence of interface sliding on the response of a layered viscoelastic pavement are presented through the analysis of a numerical example (Section 4). Several velocities are also tested to examine the effect of viscoelasticity. Finally, concluding remarks are given in Section 5.

2. Governing equations

A layered half-space composed of n horizontal layers is considered (Fig. 1). A given layer i of thickness d_i has either an elastic or a viscoelastic behavior. A moving load is applied on the free surface of the medium at a constant velocity (V); this load moves in the x direction. The problem is governed by the elastodynamic equations which are considered, for each layer, in a moving basis attached to the load. One shifts from the fixed basis (x,y,z), tied to the medium, to the moving basis (X,Y,Z) by making the following change of variable:

$$x = X + Vt; \quad y = Y; \quad z = Z. \tag{1}$$

The elastodynamic equations can be written in the moving basis (X,Y,Z) and for layer i, as follows:

$$div(\boldsymbol{\sigma}_i(X,Y,Z)) = \rho_i V^2 \frac{\partial^2 \mathbf{u}_i(X,Y,Z)}{\partial X^2}, \quad i \in \{1,n\}. \tag{2}$$

$\mathbf{u}_i$ and ρ_i denote the displacement field and the density of layer i, respectively. Boundary and interlayer conditions are required to solve Eq. (2). These conditions are explained in Section 3. Concerning the constitutive equations, a brief description of the Huet–Sayegh model (Huet, 1963; Huet, 1999; Sayegh, 1965) used to represent the viscoelastic behavior of asphalt materials encountered further in this article is given below for the one-dimensional case. The extension to the tensorial constitutive law can be obtained assuming constant Poisson's ratio (υ). As shown on the schematic representation of Fig. 2, this model is represented by a purely elastic spring (E_0) (branch I) connected in parallel to two parabolic

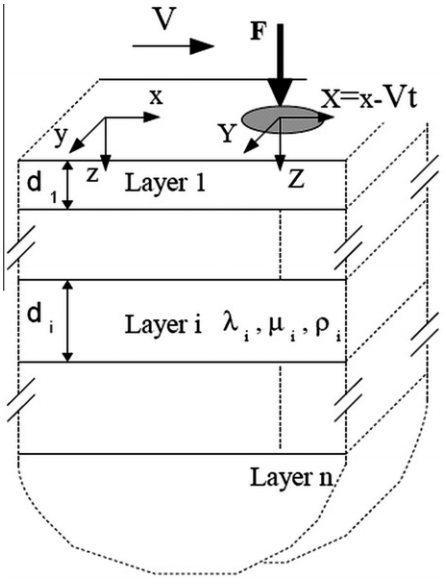

Fig. 1. Description of the moving load on a multilayered medium problem.

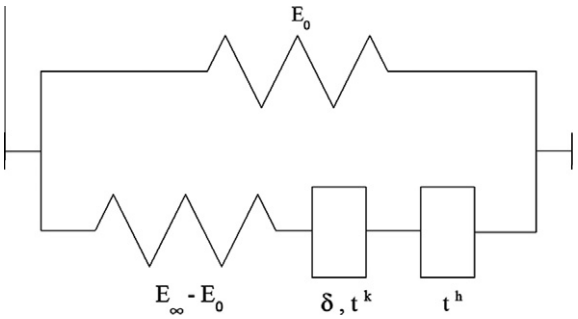

Fig. 2. Schematic representation of the Huet–Sayegh rheological model.

dampers in series with an elastic spring ($E_\infty - E_0$) (branch II). The stress–strain ($\sigma - \varepsilon$) relation for this model reads in the temporal domain:

$$\sigma(t) = E_0\varepsilon(t) + \sigma_{II}(t) \tag{3}$$

with ε and σ_{II} (stress in branch II) linked through the convolution law given below:

$$\varepsilon(t) = \int_{-\infty}^{t} F\left(\frac{t-\xi}{\tau(\theta)}\right)\frac{d}{dt}\sigma_{II}(\xi)d\xi \tag{4}$$

in which F is the creep function that reads:

$$F\left(\frac{t}{\tau(\theta)}\right) = \frac{1}{E_\infty - E_0}\quad 1 + \delta\frac{(t/\tau(\theta))^k}{\Gamma(k+1)} + \frac{(t/\tau(\theta))^h}{\Gamma(h+1)}\Big). \tag{5}$$

$\Gamma$is the Gamma function. E_0 is the static elastic modulus, $E_\infty - E_0$ is the instantaneous elastic modulus, k and h are exponents of the parabolic dampers ($1 > h > k > 0$), and δ is a positive non-dimensional coefficient balancing the contribution of the first damper in the global behavior. θ denotes temperature and τ is a response time parameter which accounts for the equivalence principle between frequency and temperature. τ is governed by:

$$\tau(\theta) = \exp(A_0 + A_1\theta + A_2\theta^2), \tag{6}$$

where A_0, A_1 and A_2 are constant parameters.

In the frequency domain in which asphalt materials are characterized, the complex modulus of the Huet–Sayegh model reads:

$$E^*(\omega\tau(\theta)) = E_0 + \frac{E_\infty - E_0}{1 + \delta(i\omega\tau(\theta))^{-k} + (i\omega\tau(\theta))^{-h}}. \tag{7}$$

The representation of the Huet–Sayegh model in the Black and Cole–Cole diagrams show that this model is able to fit accurately experimental data stemming from complex modulus tests performed on asphalt materials (Huet, 1963; Sayegh, 1965; Heck et al., 1998).

3. Semi-analytical solution of the viscoelastic multilayered half-space

A solution is first sought in the frequency domain prior to applying the inverse Fourier's transform that leads to the solution in the spatial coordinate system. A spectral method is also used in Nguyen (2002), Ricci et al. (2005).

3.1. Solution in the frequency domain

To obtain a semi-analytical solution of the aforementioned mechanical problem, the Fourier transform is applied to the displacement field in the X and Y directions and a solution is sought in the frequency domain. The bidimensional Fourier transform of the displacement field is denoted $\mathbf{u}^*$ and is given by Eq. (8):

$$\mathbf{u}^*(k_1,k_2,Z) = \int_{-\infty}^{\infty}\int_{-\infty}^{\infty}\mathbf{u}(X,Y,Z)e^{-jk_1X}e^{-jk_2Y}\,dX\,dY, \tag{8}$$

where k_1 and k_2 are the wave numbers and j is the imaginary unit. The constitutive law for viscoelastic materials is expressed in the frequency domain as follows:

$$\boldsymbol{\sigma}^*(k_1,k_2,Z) = 2\mu^*(k_1V)\boldsymbol{\varepsilon}^*(k_1,k_2,Z) + \lambda^*(k_1V)\mathrm{tr}(\boldsymbol{\varepsilon}^*(k_1,k_2,Z))\mathbf{I}. \tag{9}$$

The complex Lame coefficients, $\lambda^*(k_1V)$ and $\mu^*(k_1V)$, depend on the complex modulus $E^*(k_1V)$ in the same way as in the elastic case. $\boldsymbol{\sigma}^*$ and $\boldsymbol{\varepsilon}^*$ are the Cauchy stress and the strain tensors expressed in the frequency domain. $\mathbf{I}$ is the identity. Then, the equilibrium equation (2) can be rewritten in the frequency domain:

$$\mathbf{A}_i\frac{\partial^2\mathbf{u}^*(k_1,k_2,Z)}{\partial Z^2} + j\mathbf{B}_i\frac{\partial\mathbf{u}^*(k_1,k_2,Z)}{\partial Z} - \mathbf{C}_i\mathbf{u}^*(k_1,k_2,Z) = 0, \quad i\in\{1,n\}. \tag{10}$$

Eq. (10) applies to each layer i of the multilayered half-space and matrices $\mathbf{A}_i$, $\mathbf{B}_i$and $\mathbf{C}_i$ are given by:

$$\mathbf{A}_i = \begin{pmatrix} c_{si}^2 & 0 & 0\\ 0 & c_{si}^2 & 0\\ 0 & 0 & c_{pi}^2\end{pmatrix},$$

$$\mathbf{B}_i = \begin{pmatrix} 0 & 0 & k_1\left(c_{pi}^2 - c_{si}^2\right)\\ 0 & 0 & k_2\left(c_{pi}^2 - c_{si}^2\right)\\ k_1\left(c_{pi}^2 - c_{si}^2\right) & k_2\left(c_{pi}^2 - c_{si}^2\right) & 0\end{pmatrix},$$

$$\mathbf{C}_i = \begin{pmatrix} k_1^2\left(c_{pi}^2 - V^2\right) + k_2^2c_{si}^2 & k_1k_2\left(c_{pi}^2 - c_{si}^2\right) & 0\\ k_1k_2\left(c_{pi}^2 - c_{si}^2\right) & k_1^2\left(c_{si}^2 - V^2\right) + k_2^2c_{pi}^2 & 0\\ 0 & 0 & k_1^2\left(c_{si}^2 - V^2\right) + k_2^2c_{si}^2\end{pmatrix}, \tag{11}$$

where, in layer i, c_{pi} and c_{si} are the dilatation and the shear wave velocities whose expressions are detailed in Eq. (12).

$$c_{pi} = \sqrt{\frac{\lambda_i^* + 2\mu_i^*}{\rho_i}}, \quad c_{si} = \sqrt{\frac{\mu_i^*}{\rho_i}}. \tag{12}$$

A solution to the differential equation (10) takes the exponential form shown in Eq. (13).

$$\mathbf{u}^*(k_1,k_2,Z) = \hat{\mathbf{u}}(k_1,k_2)e^{jk_3Z}. \tag{13}$$

Seeking solutions having the form exhibited in Eq. (13) leads in turn to the determination of eigenvalues and eigenvectors of the following quadratic problem:

$$\left(k_3^2\mathbf{A}_i + k_3\mathbf{B}_i + \mathbf{C}_i\right)\hat{\mathbf{u}}(k_1,k_2) = \mathbf{0}. \tag{14}$$

Non-trivial solutions to Eq. (14) are given by Eq. (15):

$$\begin{aligned} k_3 &= \pm j\kappa_{pi},\\ k_3 &= \pm j\kappa_{si},, \end{aligned} \tag{15}$$

where κ_{pi} and κ_{si} are the longitudinal and the shear wave numbers given by:

$$\kappa_{pi} = \sqrt{\left(1 - m_{pi}^2\right)k_1^2 + k_2^2},$$

$$\kappa_{si} = \sqrt{(1 - m_{si}^2)k_1^2 + k_2^2}\quad \text{with } m_{pi}^2 = \frac{V^2}{c_{pi}^2},\ m_{pi}^2 = \frac{V^2}{c_{si}^2}. \tag{16}$$

m_{pi} and m_{si} are the Mach numbers of layer i. The eigenvectors associated to the eigenvalues obtained in Eq. (15) are:

$$\hat{\mathbf{u}}_1 = \begin{bmatrix} k_1 \\ k_2 \\ j\kappa_{pi} \end{bmatrix}, \quad \hat{\mathbf{u}}_2 = \begin{bmatrix} k_1 \\ k_2 \\ -j\kappa_{pi} \end{bmatrix}, \quad \hat{\mathbf{u}}_3 = \begin{bmatrix} 0 \\ \kappa_{si} \\ jk_2 \end{bmatrix}, \quad \hat{\mathbf{u}}_4 = \begin{bmatrix} 0 \\ -\kappa_{si} \\ jk_2 \end{bmatrix},$$
$$\hat{\mathbf{u}}_5 = \begin{bmatrix} \kappa_{si} \\ 0 \\ jk_1 \end{bmatrix}, \quad \hat{\mathbf{u}}_6 = \begin{bmatrix} -\kappa_{si} \\ 0 \\ jk_1 \end{bmatrix}. \tag{17}$$

The two first eigenvectors are linked to κ_{pi} while the others are associated to κ_{si}. Finally, the solution to Eq. (10) can be computed for each layer i ($i \in \{1,n\}$) as the sum of these eigenvectors what leads to the following expressions of the displacement field in the frequency domain:

$$\begin{aligned} u^*_{1i}(k_1,k_2,Z) &= k_1\beta^-_{1i}e^{-\kappa_{pi}Z} + \kappa_{si}\beta^-_{3i}e^{-\kappa_{si}Z} + k_1\beta^+_{1i}e^{\kappa_{pi}Z} - \kappa_{si}\beta^+_{3i}e^{\kappa_{si}Z}, \\ u^*_{2i}(k_1,k_2,Z) &= k_2\beta^-_{1i}e^{-\kappa_{pi}Z} + \kappa_{si}\beta^-_{2i}e^{-\kappa_{si}Z} + k_2\beta^+_{1i}e^{\kappa_{pi}Z} - \kappa_{si}\beta^+_{2i}e^{\kappa_{si}Z}, \\ u^*_{3i}(k_1,k_2,Z) &= j\kappa_{pi}\beta^-_{1i}e^{-\kappa_{pi}Z} + jk_2\beta^-_{2i}e^{-\kappa_{si}Z} + jk_1\beta^-_{3i}e^{-\kappa_{si}Z} \\ &\quad - j\kappa_{pi}\beta^+_{1i}e^{\kappa_{pi}Z} + jk_2\beta^+_{2i}e^{\kappa_{si}Z} + jk_1\beta^+_{3i}e^{\kappa_{si}Z}. \end{aligned} \tag{18}$$

The displacement field logically depends on the wave numbers and the Z-coordinate. It also involves six constant parameters per layer which are called amplitudes (Eq. (19)):

$$\boldsymbol{\beta}_i = \begin{bmatrix} \boldsymbol{\beta}^-_i \\ \boldsymbol{\beta}^+_i \end{bmatrix}, \quad \text{with } \boldsymbol{\beta}^-_i = \begin{pmatrix} \beta^-_{1i} \\ \beta^-_{2i} \\ \beta^-_{3i} \end{pmatrix} \text{ and } \boldsymbol{\beta}^+_i = \begin{pmatrix} \beta^+_{1i} \\ \beta^+_{2i} \\ \beta^+_{3i} \end{pmatrix}. \tag{19}$$

For the whole multilayered medium, $6n$ parameters have to be determined from boundary conditions. To accomplish this, contact conditions expressed at the interface between layers are required. These contact laws involve displacements or/and stresses. For use in the interlayer conditions, the traction vector (Eq. (20)) of layer i ($i \in \{1,n\}$), corresponding to the normal e_Z, is defined from Eq. (18) and the constitutive relation Eq. (9).

$$\begin{aligned} \sigma^*_{13i} &= \mu^*_i\Big[-2k_1\kappa_{p_i}\beta^-_{1i}e^{-\kappa_{pi}Z} - k_1k_2\beta^-_{2i}e^{-\kappa_{si}Z} - \left(k_1^2+\kappa_{si}^2\right)\beta^-_{3i}e^{-\kappa_{si}Z} \\ &\quad + 2k_1\kappa_{pi}\beta^+_{1i}e^{\kappa_{pi}Z} - k_1k_2\beta^+_{2i}e^{\kappa_{si}Z} - \left(k_1^2+\kappa_{si}^2\right)\beta^+_{3i}e^{\kappa_{si}Z}\Big], \\ \sigma^*_{23i} &= \mu^*_i\Big[-2k_2\kappa_{pi}\beta^-_{1i}e^{-\kappa_{pi}Z} - \left(k_2^2+\kappa_{si}^2\right)\beta^-_{2i}e^{-\kappa_{si}Z} - k_1k_2\beta^-_{3i}e^{-\kappa_{si}Z} \\ &\quad + 2k_2\kappa_{pi}\beta^+_{1i}e^{\kappa_{pi}Z} - \left(k_2^2+\kappa_{si}^2\right)\beta^+_{2i}e^{\kappa_{si}Z} - k_1k_2\beta^+_{3i}e^{\kappa_{si}Z}\Big], \\ \sigma^*_{33i} &= j\mu^*_i\Big[-\left(k_1^2+k_2^2+\kappa_{si}^2\right)\beta^-_{1i}e^{-\kappa_{pi}Z} - 2k_2\kappa_{si}\beta^-_{2i}e^{-\kappa_{si}Z} \\ &\quad - 2k_1\kappa_{si}\beta^-_{3i}e^{-\kappa_{si}Z} - \left(k_1^2+k_2^2+\kappa_{si}^2\right)\beta^+_{1i}e^{\kappa_{pi}Z} + 2k_2\kappa_{si}\beta^+_{2i}e^{\kappa_{si}Z} + 2k_1\kappa_{si}\beta^+_{3i}e^{\kappa_{si}Z}\Big]. \end{aligned} \tag{20}$$

3.2. Determination of the amplitude vector

The amplitude vector is determined from boundary conditions at the free surface and at infinity as well as from the interlayer contact conditions.

Boundary conditions on the free surface and at infinity yield six equations. At the free surface the condition reads:

$$\boldsymbol{\sigma}^*_{Z=0} \cdot \mathbf{e}_Z = \hat{\mathbf{f}}, \tag{21}$$

where $\hat{\mathbf{f}}$ is the Fourier transform of the imposed force vector. The radiation condition is considered at infinity, in the underlying half-space, so that the displacement field must scatter to infinity. Given the displacement response shown in Eq. (18) the radiation condition implies that $\boldsymbol{\beta}^+_n$ is equal to zero at infinity.

The contact conditions at the interface between layers provide $6(n-1)$ equations (six equations per interface). Two types of condition are analyzed in this article: the continuity (or bonded) and the interface sliding conditions. The continuity condition is commonly used and states that the displacements and the traction vector from both sides of an interface are equal at the Z-coordinate of this interface. This condition for an interface located between layers i and $i+1$ reads:

$$\begin{bmatrix} \mathbf{u}^*(k_1,k_2,Z) \\ \boldsymbol{\sigma}^*(k_1,k_2,Z)\cdot\mathbf{e}_Z \end{bmatrix}_i = \begin{bmatrix} \mathbf{u}^*(k_1,k_2,Z) \\ \boldsymbol{\sigma}^*(k_1,k_2,Z)\cdot\mathbf{e}_Z \end{bmatrix}_{i+1}. \tag{22}$$

On the other hand, the sliding condition stipulates that the shear components of the traction vector are equal to zero at both sides of an interface. In the same time, the conditions on the vertical displacement and the third component of the traction vector remain the same as in Eq. (22). The sliding case for an interface settled between layers i and $i+1$ reads:

$$\begin{pmatrix} u^*_3(k_1,k_2,Z) \\ \sigma^*_{13}(k_1,k_2,Z) \\ \sigma^*_{23}(k_1,k_2,Z) \\ 0 \\ 0 \\ \sigma^*_{33}(k_1,k_2,Z) \end{pmatrix}_i = \begin{pmatrix} u^*_3(k_1,k_2,Z) \\ 0 \\ 0 \\ \sigma^*_{13}(k_1,k_2,Z) \\ \sigma^*_{23}(k_1,k_2,Z) \\ \sigma^*_{33}(k_1,k_2,Z) \end{pmatrix}_{i+1}. \tag{23}$$

Accounting for interface relations plus the boundary conditions at the top layer and at infinity leads to a well-defined problem of $6n$ unknowns and $6n$ equations.

The global matrix technique (Schmidt and Tango, 1986) is adopted to calculate the amplitude vector which is obtained by solving a unique linear system per couple of wave numbers (k_1,k_2). This method enables to easily handle the combination of bonded and sliding interfaces of a multilayered structure. The assembly of the global matrix relies on Eq. (24) that links quantities of layer i and $i+1$ at the interface between these two layers.

$$(\mathbf{M}_i\bar{\mathbf{e}}_i)\cdot\boldsymbol{\beta}_i = (\mathbf{N}_{i+1})\cdot\boldsymbol{\beta}_{i+1}, \quad i \in \{1,n\}. \tag{24}$$

$\mathbf{M}_i$ and $\mathbf{N}_{i+1}$ are 6-by-6 matrices that depend on the material properties of layer i and $i+1$, respectively. These matrices are different from sliding to bonded interfaces. Substitution of Eqs. (18) and (20) in Eq. (22) leads to the determination of matrices $\mathbf{M}_i$ and $\mathbf{N}_i$ in the bonded case. The definition of $\mathbf{M}_i$ and $\mathbf{N}_i$ for sliding interfaces is obtained by inserting Eqs. (18) and (20) into Eq. (23). These matrices are detailed in the appendix for both cases. $\bar{\mathbf{e}}_i$ is a diagonal 6-by-6 matrix that compiles the exponential terms of displacements and stresses involved in the contact relations. $\bar{\mathbf{e}}_i$ is defined as follows:

$$\mathrm{diag}(\bar{\mathbf{e}}_i) = \begin{bmatrix} e^{-\kappa_{pi}d_i} & e^{-\kappa_{si}d_i} & e^{-\kappa_{si}d_i} & e^{\kappa_{pi}d_i} & e^{\kappa_{si}d_i} & e^{\kappa_{si}d_i} \end{bmatrix}^T, \tag{25}$$

where the exponential terms are computed at the Z-coordinates of interfaces only. To formulate the contact conditions at an interface, a change of variable is locally operated: for each layer, the origin of the Z-axis is chosen at the top of the considered layer. As a consequence, for an interface located between layers i and $i+1$, the Z-coordinate of this interface is $Z = d_i$ for layer i and $Z = 0$ for layer $i+1$. This change of variable explains why no exponential term appears in the left hand side of Eq. (24). $\bar{\mathbf{e}}_i$ does not depend on the type of interface.

To obtain the amplitude vector, one needs to solve the linear system above (Eq. (26)) in which the assembled matrix is block diagonal.

$$\begin{bmatrix} \mathbf{D}_0 & & & & & \\ \mathbf{M}_1\overline{e_1} & -\mathbf{N}_2 & & & \mathbf{0} & \\ & \mathbf{M}_2\overline{e_2} & -\mathbf{N}_3 & & & \\ & & \ddots & & & \\ & & & \mathbf{M}_i\overline{e_i} & -\mathbf{N}_{i+1} & \\ & \mathbf{0} & & & \ddots & \\ & & & & \mathbf{M}_{n-1}\overline{e_{n-1}} & -\mathbf{D}_n \end{bmatrix} \begin{Bmatrix} \begin{bmatrix}\boldsymbol{\beta}_1^- & \boldsymbol{\beta}_1^+\end{bmatrix}^T \\ \begin{bmatrix}\boldsymbol{\beta}_2^- & \boldsymbol{\beta}_2^+\end{bmatrix}^T \\ \vdots \\ \vdots \\ \begin{bmatrix}\boldsymbol{\beta}_i^- & \boldsymbol{\beta}_i^+\end{bmatrix}^T \\ \vdots \\ \boldsymbol{\beta}_n^- \end{Bmatrix} = \begin{Bmatrix} \hat{\mathbf{f}} \\ \mathbf{0} \\ \vdots \\ \vdots \\ \vdots \\ \vdots \\ \mathbf{0} \end{Bmatrix}. \tag{26}$$

The filling procedure of the global matrix bears on the repetition of Eq. (24) for every interface. Eq. (26) is verified whatever the interface condition. The first block of the global matrix is the 3-by-6 matrix, $\mathbf{D}_0$. It reflects the boundary condition at the free surface (Eq. (21)). $\mathbf{D}_0$ is given in the appendix. On the other hand, the boundary condition at infinity affects the last block ($\mathbf{D}_n$) whose size is 6-by-3 instead of 6-by-6. $\boldsymbol{\beta}_n^+$ is indeed equal to zero so it is not included in the unknown vector ($\boldsymbol{\beta}$). $\mathbf{D}_n$ is equivalent to $\mathbf{M}_n^-$ for the bonded condition whereas it is equal to $\mathbf{N}_n^-$ for sliding interfaces. The size of the global matrix is $6(n-1)+3$. Naturally, different conditions can be mixed within the global matrix.

Before solving the linear system (Eq. (26)) by using a pivoting method, two particular treatments must be applied to this system. In the global matrix, indeed, some terms relate to the displacement field and others to the stress field. The order of magnitude of these fields may be significantly different leading to a global matrix that is ill conditioned. To overcome this difficulty, the terms that connect to the stress field are divided by the module of the μ^* Lame coefficient. These terms are exactly divided by the largest module of μ_i^* and μ_{i+1}^* providing that the interface between layers i and $i+1$ is concerned. This treatment applies for both the perfect-slip interface condition (Eq. (23)) and the bonded condition (Eq. (22)). The same operation must be employed on the right hand side of Eq. (26) so $\hat{f}$ is divided by $\max(|\mu_1^*|,|\mu_2^*|)$ whatever are the interface conditions within the structure. A second treatment is necessary when the positive exponentials in $\bar{e}_i$ become too large, i.e. large values of N_1 and N_2 are required to perform the FFT (Section 3.3), triggering overflow issues. These exponentials depend on either κ_{pi} or κ_{si} which themselves are function of k_1 and k_2. A change of variable is made to get over this second difficulty: the positive exponentials in Eq. (25) are divided by $\exp\left(\sqrt{k_1^2+k_2^2}\right)d_i$ and so are the β_i^+ once the system of Eq. (26) has been solved. Note that the particular treatments mentioned above follow the recommendation of the specialized literature in terms of stability of the numerical solution. In particular, according to Schmidt and Tango (1986), unconditionally stable solutions can be ensured by using Gaussian elimination with partial pivoting, where only simple scaling and rearrangement is employed.

We implemented the method presented in this section as well as the different interface conditions in the ViscoRoute kernel (Duhamel et al., 2005) which uses the C++ language programming.

3.3. Solution in the spatial domain

The solution of Eq. (2) in the spatial domain (X,Y,Z) is obtained by integration of its counterpart in the frequency domain (k_1,k_2,Z). The integration is not straightforward because of the form of the integrand that leads to improper integrals. Several difficulties arise: either the integrand is not directly defined from a numerical viewpoint at some (k_1,k_2) but it is continuous and finite at those points, or the integrand is infinite at some (k_1,k_2) within the integration interval but still integrable (integrable singularity). Moreover, in the vicinity of those critical points, the integrand varies rapidly causing accuracy issues of the numerical integration.

These difficulties can be illustrated in the case of a homogeneous half-space in which, for instance, the vertical displacement in the frequency domain reads:

$$u_3^*(k_1,k_2,Z)=\frac{e^{-(\kappa_p+\kappa_s)Z}\kappa_p f_Z\left(-2e^{\kappa_p Z}\left(k_1^2+k_2^2\right)+e^{\kappa_s Z}\left(k_1^2+k_2^2+\kappa_s^2\right)\right)}{\mu^*\left(\left(k_1^2+k_2^2\right)^2-4\left(k_1^2+k_2^2\right)\kappa_p\kappa_s+2\left(k_1^2+k_2^2\right)\kappa_s^2+\kappa_s^4\right)}. \tag{27}$$

f_Z, which is supposed to be well-defined, is the applied force at the surface of the medium. The first difficulty with Eq. (27) comes up when $k_1=0$ and $k_2\neq 0$ because in this case the denominator is zero. However, the Taylor series expansion at about $k_1=0$ and $k_2\neq 0$ of the displacement u_3^* is:

$$u_3^*(k_1,k_2,Z)=-\frac{e^{-k_2 Z}f_Z\left(-k_2^2m_p^2Z+m_s^2\left(k_2+k_2^2Z\right)\right)}{2\mu^*\left(k_2^2\left(m_p^2-m_s^2\right)\right)}+\mathrm{O}[k_1]^2. \tag{28}$$

In the case of a homogeneous half-space, the vertical displacement could be replaced by Eq. (28) when $k_1=0$ and $k_2\neq 0$. This is not feasible for a multilayered structure. Here, m_p is different from m_s, and u_3^* is singular or not depending on the value of μ^*. For the Huet–Sayegh model which is used in the numerical example of the present article and briefly described in Section 2, μ^* is defined in the wavenumber domain as follows:

$$\mu^*(k_1V,\theta)=\frac{1}{2(1+\upsilon)}\quad E_0+\frac{E_\infty-E_0}{1+\delta(ik_1V\tau(\theta))^{-k}+(ik_1V\tau(\theta))^{-h}}\Bigg). \tag{29}$$

E_0 cannot be equal to zero and therefore μ^* is never nil. However, since for usual data E_0 is very small compared to E_∞, μ^* strongly varies with k_1 in the vicinity of $k_1=0$ whatever is k_2. μ^* is close to a function of the form k_1^h as long as k_1 is small and different from zero. This generates accuracy troubles in the numerical integration although u_3^* is not singular.

On the other hand, the Taylor series at about $k_1=k_2=0$ of u_3^* reads:

$$u_3^*(k_1,k_2,Z)=\frac{a^2f_Zm_s^2\sqrt{b^2-a^2\left(m_p^2-1\right)}}{-\left(-2b^2+a^2\left(m_s^2-2\right)\right)^2+4\left(a^2+b^2\right)\sqrt{b^2-a^2\left(m_p^2-1\right)}\sqrt{b^2-a^2\left(m_s^2-1\right)}}\cdot\frac{1}{\mu^*\varepsilon}+\frac{C(a,b,Z)}{\mu^*}+\mathrm{O}[\varepsilon]. \tag{30}$$

In the above equation, we set $k_1=a\varepsilon$, $k_2=b\varepsilon$ and the Taylor series was developed around $\varepsilon=0$. $C(a,b,Z)$ is a function of a, b and Z. This time, the vertical displacement in the frequency domain is singular in $\varepsilon=0$, and the integrable singularity takes the form $1/\varepsilon$ which is typical of the purely elastic problem. Note that in elasticity there is no singularity in $k_1=0$, $k_2\neq 0$. The issue concerning μ^* is similar to that explained previously.

The generalization of the above analysis to a multilayered structure could be done through the development in Taylor series of the algebraic system that defines the solution in the frequency domain for multilayered media. This is not formulated herein.

In conclusion, two types of improper integrals encountered when computing the solution in the spatial domain have been described. The mentioned difficulties appear in $k_1 = 0$, $k_2 \neq 0$ and $k_1 = k_2 = 0$. To overcome these obstacles a specific scheme of integration is envisaged. To explain this scheme, let $\hat{g}(k_1, k_2, Z)$ denote the function to integrate. Then, the integrated function $g(X,Y,Z)$ that represents a component of the displacement, the stress or the strain field in the spatial coordinate system takes the form:

$$\begin{aligned} g(X,Y,Z) &= \frac{1}{4\pi^2}\int_{-\infty}^{\infty}\int_{-\infty}^{\infty}\hat{g}(k_1,k_2,Z)e^{ik_1X}e^{ik_2Y}\,dk_1\,dk_2 \\ &\approx \frac{1}{4\pi^2}\left[\delta k_1\delta k_2 \mathrm{FFT}_{2D}[(1-Ind(k_1))\hat{g}(k_1,k_2,Z)]\right. \\ &\quad \left. + \int_{-\infty}^{\infty}\int_{-\infty}^{\infty}[Ind(k_1)\hat{g}(k_1,k_2,Z)e^{ik_1X}e^{ik_2Y}\,dk_1\,dk_2]\right] \\ &\approx \frac{1}{4\pi^2}\left[\delta k_1\delta k_2 \mathrm{FFT}_{2D}[(1-Ind(k_1))\hat{g}(k_1,k_2,Z)]\right. \\ &\quad \left. + \int_{-\infty}^{\infty}\int_{H(\delta k_1)}\hat{g}(k_1,k_2,Z)e^{ik_2Y}\,dk_1\,dk_2\right]. \end{aligned} \tag{31}$$

FFT_{2D} denotes the two-dimensional Fast Fourier Transform. $Ind(k_1)$ and $Ind(k_2)$ are the interval indicator functions such that:

$$Ind(k_1) = \begin{cases} 1, & k_1 \in H(\delta k_1) = [-\delta k_1/2, \delta k_1/2] \\ 0, & k_1 \notin H(\delta k_1) \end{cases} \quad \text{and}$$
$$Ind(k_2) = \begin{cases} 1, & k_2 \in H(\delta k_2) = [-\delta k_2/2, \delta k_2/2] \\ 0, & k_2 \notin H(\delta k_2) \end{cases} \tag{32}$$

The exponential term e^{ik_1X} is neglected in the evaluation of the last term of Eq. (31) for which k_1 is close to zero. Similarly, e^{ik_2Y} is neglected in the last term of Eq. (33) which is obtained by decomposition of Eq. (31)

$$\begin{aligned} g(X,Y,Z) \approx{}& \frac{1}{4\pi^2}[\delta k_1\delta k_2 \mathrm{FFT}_{2D}[(1-Ind(k_1))\hat{g}(k_1,k_2,Z)] \\ &+ \delta k_2 \mathrm{FFT}_{k_2}\left[(1-Ind(k_2))\int_{H(\delta k_1)}\hat{g}(k_1,k_2,Z)dk_1\right] \\ &+ \int_{H(\delta k_2)}\int_{H(\delta k_1)}\hat{g}(k_1,k_2,Z)dk_1\,dk_2\Big]. \end{aligned} \tag{33}$$

FFT_{k_2} denotes the one-dimensional FFT in the k_2-direction. Practically, the last integral within the brackets of Eq. (33) leads to a constant which is inserted in the array of the FFT_{k_2} discrete values in $k_2 = 0$. This constant is divided by δk_2 prior to insertion. Eq. (33) indicates that to obtain $g(X,Y,Z)$, we first perform a 2D FFT on the whole domain minus a small strip centered in $k_1 = 0$. Two other integrations are then performed over the domain omitted in the 2D FFT. This decomposition enables to handle the aforementioned integration issues. The results of these integrations, which are detailed below, are added to compose the solution in the spatial domain.

3.3.1. Calculation of $\mathrm{FFT}_{2D}[(1-Ind(k_1))\hat{g}(k_1,k_2,Z)]$

To perform the 2D FFT, the solution in the frequency domain, which is a continuous function of k_1 and k_2, is discretized within the range of integration that goes from $-N_1\delta k_1/2$ to $N_1\delta k_1/2$ in the k_1-direction and from $-N_2\ \delta k_2/2$ to $N_2\delta k_2/2$ in the k_2-direction. The steps of discretization or sampling intervals are denoted δk_1 and δk_2. N_1 and N_2 are determined by ensuring that discrete values of the solution in the frequency domain are negligible for sufficiently large values of k_1 and k_2, respectively. The criterion used to evaluate N_1 reads:

$$\sum_{i_1=1}^{i_1=5}\left|\hat{g}\left(-\frac{N_1}{2}\delta k_1 + i_1\delta k_1, 0, Z\right)\right| < \varepsilon\sum_{i_1=1}^{i_1=5}|\hat{g}(i_1\delta k_1, 0, Z)|, \tag{34}$$

where ε is a small positive quantity. $\hat{g}(k_1,k_2,Z)$ is supposed to be non-zero only in a finite interval of k_1 and k_2 that is itself supposed to be contained within the range of integration. Eq. (34) checks that the aforesaid statement is verified with a good accuracy; the same technique is used to set N_2. Note that prior to running the 2D FFT, $\hat{g}(k_1,k_2,Z)$ is set equal to zero in $k_1 = 0$.

3.3.2. Calculation of $\mathrm{FFT}_{k_2}[(1-Ind(k_2))\int_{H(\delta k_1)}\hat{g}(k_1,k_2,Z)dk_1]$

It is achieved in two steps. A Gauss quadrature is first used before an one-dimensional FFT is applied in the k_2-direction. The interval $H(\delta k_1)$ is split into two subintervals: $[-\delta k_1/2, 0]\cup]0, \delta k_1/2]$, and seven points are used on each subintervals to perform the Gauss quadrature. The following change of variable is made prior to the Gaussian integration:

$$k_1 = \left(\frac{1+x}{2}\right)^3\frac{\delta k_1}{2} \tag{35}$$

and finally the integral over $H(\delta k_1)$ is computed as follows:

$$\begin{aligned} \int_{H(\delta k_1)}\hat{g}(k_1,k_2,Z)dk_1 = \sum_{i=1}^{7}\frac{3\delta k_1}{4}w_i\left(\frac{1+x_i}{2}\right)^2 \\ \times\left[\hat{g}\left(k_1^i,k_2,Z\right)+\hat{g}\left(-k_1^i,k_2,Z\right)\right]. \end{aligned} \tag{36}$$

x_i and w_i are the abscissas and the weights of the Gauss–Legendre quadrature rule, and k_1^i are the discrete values at which $\hat{g}$ is computed. These are obtained from Eq. (35) for $x = x_i$. Eq. (36) is calculated for the k_2 discrete values going from $-N_2\delta k_2/2$ to $N_2\delta k_2/2$. The integrated function for all k_2 discrete values is stored in an array in which real and imaginary parts alternate. This array is then used to perform the one-dimensional FFT in the k_2 direction. The value of this array for the zero frequency is obtained from the integration described in Section 3.3.3.

3.3.3. Calculation of $\int_{H(\delta k_1)}\int_{H(\delta k_2)}\hat{g}(k_1,k_2,Z)dk_1\,dk_2$

A similar procedure to the one exposed above is used to compute this integral. This leads to the formula:

$$\begin{aligned} \int_{H(\delta k_2)}\int_{H(\delta k_1)}\hat{g}(k_1,k_2,Z)dk_1\,dk_2 = 2*\sum_{j=1}^{7}\sum_{i=1}^{7}\frac{9\delta k_1\delta k_2}{16}w_jw_i\left(\frac{1+x_j}{2}\right)^2 \\ \times\left(\frac{1+x_i}{2}\right)^2\left[\hat{g}\left(k_1^i,k_2^i,Z\right)\right. \\ \left.+\hat{g}\left(-k_1^i,k_2^i,Z\right)\right]. \end{aligned} \tag{37}$$

The following symmetry, related to the one existing in the y-direction of the spatial domain, is used in Eq. (37): $\hat{g}(k_1,k_2) = \hat{g}(k_1,-k_2)$.

Once all the aforementioned integrations have been performed and added to obtain a solution in the spatial domain, another criterion is checked. It verifies that the continuous function has been properly sampled and that aliasing effects (owing to non-adapted sampling frequencies) have been minimized. This second criterion in the k_1-direction reads:

$$\sum_{i_1=1}^{i_1=5}\left|g\left(-\frac{N_1}{2}\delta x_1 + i_1\delta x_1, 0, Z\right)\right| < \tilde{\varepsilon}\sum_{i_1=1}^{i_1=5}|g(i_1\delta x_1, 0, Z)|. \tag{38}$$

$\tilde{\varepsilon}$ is a small positive quantity and $\delta x_1 = 2\pi/(\delta k_1 N_1)$. If Eq. (38) is not verified the sampling interval δk_1 is divided by two and the integration process is restarted from the beginning. This procedure is run until an acceptable solution is reached. A similar verification holds for δk_2.

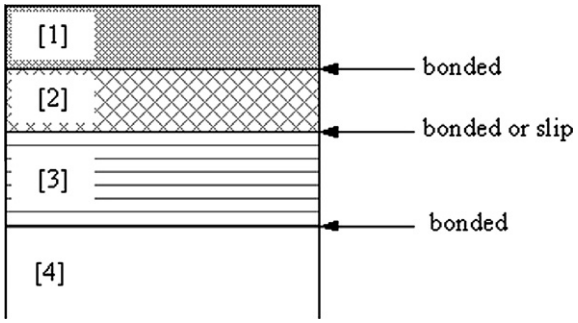

Fig. 3. Sketch of the studied multilayered pavement structure.

Table 1
Properties of the elastic layers considered in the validation case.

Layer	Thickness (m)	E (MPa)	ν	Type
[1]	0.08	5400	0.35	Bituminous material
[2]	0.12	9300	0.35	Bituminous material
[3]	0.20	23,000	0.25	Material treated with hydraulix binders
[4]	Infinite	120	0.35	Foundation

4. Numerical applications to a four-layer semi-infinite structure

This section is split into two subsections. The first one aims at validating the accuracy and the implementation of the methods detailed in Section 3. It studies a multilayered structure for which all layers have an elastic behavior. In the second subsection, the influence of interface slip on the mechanical response of the same structure but with viscoelastic layers is analyzed. The mechanical response of a structure, with bonded or sliding interfaces, to a moving load is typical of pavement problems.

The structure under consideration is described in Fig. 3. It is a composite pavement that consists of four layers defined as follows: a surface course of bituminous materials, a base layer of bituminous materials, a layer of materials treated with hydraulic binders, and a pavement foundation. As shown in Fig. 3, a sliding interface condition can be introduced between layers 2 and 3, i.e. between the asphalt and the concrete cement layers.

The layers of composite pavements are initially bonded. However, due to traffic stresses and differential expansion between the base of layer 2 and layer 3, the bonding between the asphalt concrete and the material treated with hydraulic binders may eventually fail (SETRA-LCPC, 1997). To better understand the effect of interface slip on the long-term behavior of such structures, their mechanical response to a moving load needs to be investigated by introducing sliding between these two layers.

4.1. Validation case in elasticity

The validation of the developed method is performed by comparison with software ALIZE-LCPC (Autret et al., 1982) which is used in the French design of pavements. ALIZE-LCPC computes the Burmister solution (Burmister, 1943) of an elastic multilayered half-space under static loading. This comparison enables to check the solution procedure through a global matrix, the implementation of sliding as an interface condition and the integration methods. The confrontation is performed, at different depths, on components of the displacement, the strain and the stress fields.

All layers of the studied structure are assumed to have an elastic behavior (Hooke's law) as described by the Young moduli and Poisson's ratios given in Table 1.

A uniform disc-shaped load of 0.25 m in diameter (i.e. $2a = 0.25$ m) and centered in ($X = 0$, $Y = 0$, $Z = 0$) is applied (in the Z-direction) on the free surface of the pavement structure. The pressure load, f_0, is equal to 0.662 MPa which corresponds to the value used in the French design of pavements (SETRA-LCPC, 1997). The load expression in the frequency domain is then given by Eq. (39):

$$\hat{\mathbf{f}} = \begin{pmatrix} 0 \\ 0 \\ \hat{f}_Z \end{pmatrix} \quad \text{with} \quad \hat{f}_Z = f_0 J_1\left(a\left[k_1^2 + k_2^2\right]^{1/2}\right)\delta(x_3)/a\left[k_1^2 + k_2^2\right]^{1/2}, \tag{39}$$

where J_1 is a Bessel function of the first kind.

Figs. 4 and 5 show the comparison between the results obtained from the developed method and ALIZE-LCPC when the sliding interface condition is considered between layers 2 and 3. Figs. 4(a), (b) and 5(a) display horizontal profiles (in the X-direction, $Y = 0$), at two different depths corresponding to the base of asphalt concrete ($Z_1 = 0.19$ m) and the base of materials treated with hydraulic binders ($Z_2 = 0.39$ m), of the vertical displacement, the normal stress (σ_{xx}) and the component of longitudinal strain in the direction of rolling (ε_{xx}), respectively. Only half of these profiles (in the X-direction) are plotted because of the symmetry of the mechanical response in elasticity. Fig. 5(b) shows the vertical profile (in the Z-direction) of the longitudinal strain (ε_{xx}). In all these figures, the curves obtained from the developed method perfectly match the ones stemming from ALIZE-LCPC. The developed method is thus validated and is going to be applied, in Section 4.2, to a pavement structure including viscoelastic materials. More details on the trends observed in the strain and stress profiles are also provided below.

4.2. Effects of the sliding interface condition in viscoelasticiy

In this section, two cases of interface condition are studied. Either a sliding or a bonded interface condition is assumed

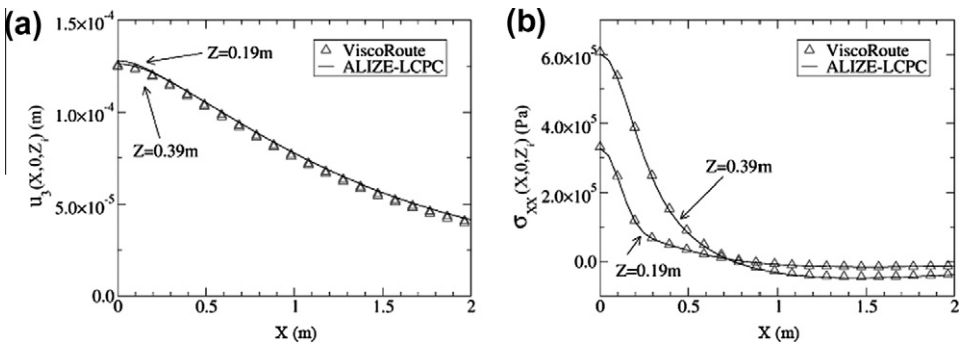

Fig. 4. Mechanical response under static loading of an elastic four-layer structure with a slip boundary between layers 2 and 3. Comparison of ViscoRoute with ALIZE-LCPC: (a) vertical displacement versus X-coordinate for two different depths and (b) normal stress in the X direction versus X-coordinate for two different depths.

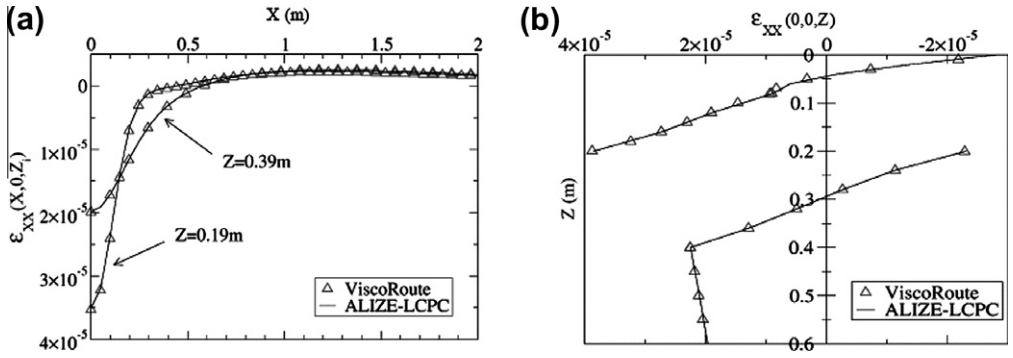

Fig. 5. Mechanical response under static loading of an elastic four-layer structure with a slip boundary between layers 2 and 3. Comparison of ViscoRoute with ALIZE-LCPC: (a) longitudinal strain versus *X*-coordinate and (b) vertical profile of the longitudinal strain.

Table 2
Properties of the pavement structure layers.

Layer	E_0 (MPa)	E_∞ (MPa)	δ	k	h	A_0	A_1	A_2	ν
[1]	11	32,665	2.24	0.19	0.59	2.943	−0.39742	1.95E−03	0.35
[2]	13	43,934	2.10	0.17	0.53	5.945	−0.39962	1.070E−03	0.35
	E (MPa)	ν							
[3]	23,000	0.25							
[4]	120	0.35							

between layers 2 and 3 of the structure depicted in Fig. 3. Moreover, the bituminous layers (layers 1 and 2) have a viscoelastic behavior described by the Huet–Sayegh model (Huet, 1963, 1999; Sayegh, 1965) which is appropriate to model the behavior of asphalt materials. In the frequency domain, the complex modulus of this model depends on the load speed and the temperature as shown in Eq. (29). The values of the Huet–Sayegh parameters corresponding to the bituminous materials involved herein are summarized in Table 2 that also gathers the elastic properties of layers 3 and 4.

The longitudinal strain (ε_{xx}) and the normal stress (σ_{xx}) are analyzed in this section. These quantities commonly intervene in the criteria for the design of pavements in France that, basically, rely on the estimate of tensile stresses and strains at particular locations in the structure (SETRA-LCPC, 1997). When a single load is applied on the pavement, the maximum tensile strain is obtained for the ε_{xx} component of the strain tensor. This is not systematically verified for multiple loads (Chabot et al., 2010).

Fig. 6 shows the longitudinal strain component (ε_{xx}) as a function of the depth in the structure for several load velocities and at a temperature of 30 °C. These vertical profiles are collected right under the load, in $X = Y = 0$. The sliding (plus markers) and the bonded (circle markers) interface conditions are compared on each graph. The temperature in the bituminous courses is constant and set to thirty degrees Celsius. Note that the temperature is used in Eq. (6) to determine the response time parameter and that the higher the temperature the more viscous is the behavior of asphalt materials. Likewise, the response of the structure depends on the load velocity due to viscoelasticity of layers 1 and 2. Low speeds lead to higher viscoelastic deformations. In Fig. 6, the load velocity ranges from 20 m/s to 0.1 m/s which is close to the static case.

As expected, the sliding interface condition enforced between layers 2 and 3 yields a discontinuity in the longitudinal strain at this location ($z = 0.2$ m). This discontinuity is noticeable in all graphs of Fig. 6. In layers 3 and 4, beneath the slip interface, ε_{xx} remains quite unchanged as the velocity varies. In these layers, a relatively small influence of the velocity on ε_{xx} is also noticed in the bonded case. Contrarily, the longitudinal strain depends strongly on the velocity in layers 1 and 2 in which, at a velocity of 20 m/s, ε_{xx} evolves almost linearly with depth. This variation becomes non-linear, essentially in the first layer, as the velocity lowers. At a velocity of 20 m/s, compressive strain is observed in the first layer whereas tensile strain prevails at velocities inferior or equal to 1 m/s.

For all studied velocities, the maximum magnitude in ε_{xx} (compressive or tensile strain) is higher for the interlayer slip condition than for the bonded condition. For $v = 20$ m/s, $v = 5$ m/s and $v = 1$ m/s, the maximum tensile strain is located in layer 2 next to the interface with layer 3. In the near static case, this maximum is observed in layer 1. At relatively high velocities ($v = 20$ m/s or $v = 5$ m/s), values of the same order of magnitude as the maximum strain for these speeds are also attained at the interface between layers 3 and 4. Then, as the velocity decreases the maximum tensile strain increases. In the near static case ($v = 0.1$ m/s), the maximum tensile strain is equal to more than twice its value at a velocity of 20 m/s. For full bonded conditions the maximum tensile strain is also located in layer 1 for velocities lesser than 1 m/s.

Besides, horizontal profiles in the X direction ($Y = 0$) of the longitudinal strain, ε_{XX}, are plotted in Figs. 7(a) and 7(b) whose curves are obtained for a velocity of 0.1 m/s and 20 m/s, respectively. These profiles are computed for a temperature of 30 °C and at a depth of 0.18 m, just above the interface between layers 2 and 3. The horizontal profiles confirm that as speed decreases the maximum magnitude in ε_{XX} increases and that the slip boundary case leads to higher longitudinal deformations. We also notice that, at a depth of 0.18 m, the bonded case yields essentially contraction strains (negative value of ε_{XX}) which are much smaller than the extension strains observed in the sliding case. Additionally, note that the maximum value of extension at a velocity of 0.1 m/s (i.e. for highly viscous materials) is located a little behind the center of the load imprint, at about 0.05 m.

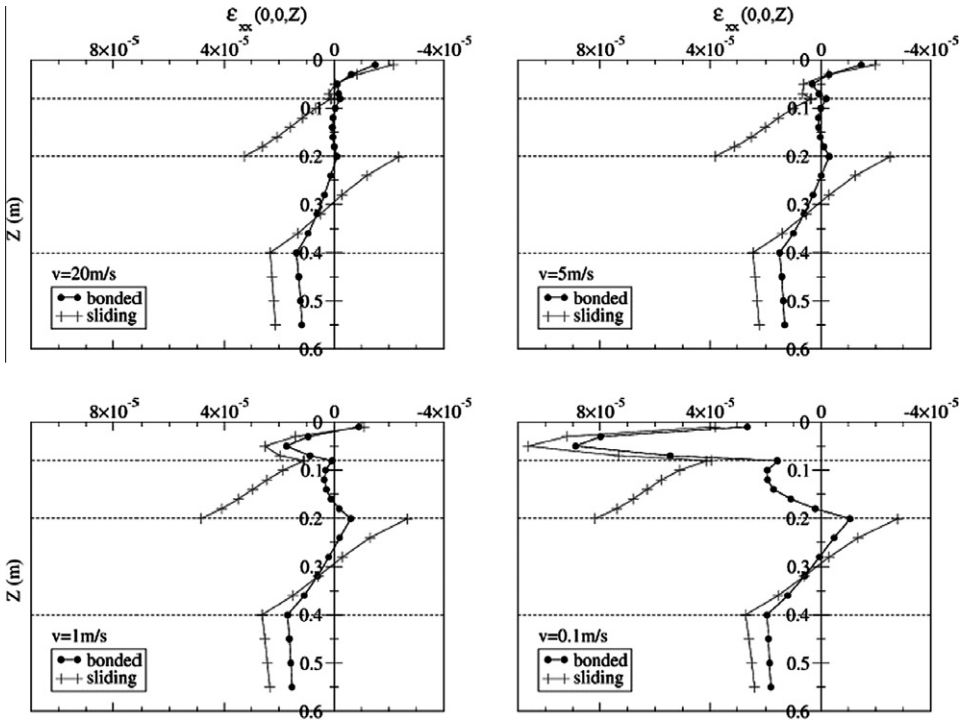

Fig. 6. Mechanical response under a moving load of a viscoelastic four-layer structure with a bonded or a slip boundary between layers 2 and 3: influence of the load velocity on the longitudinal strain (vertical profiles).

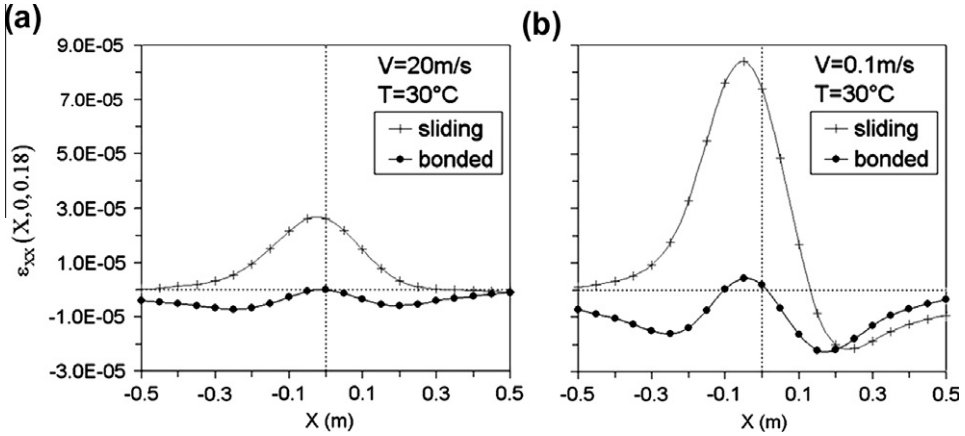

Fig. 7. Horizontal profile at a depth of 0.18 m of the longitudinal strain computed for a four-layer viscoelastic system excited by a moving load. A bonded or a slip boundary is assumed between layers 2 and 3. (a) $V = 20$ m/s and (b) $V = 0.1$ m/s.

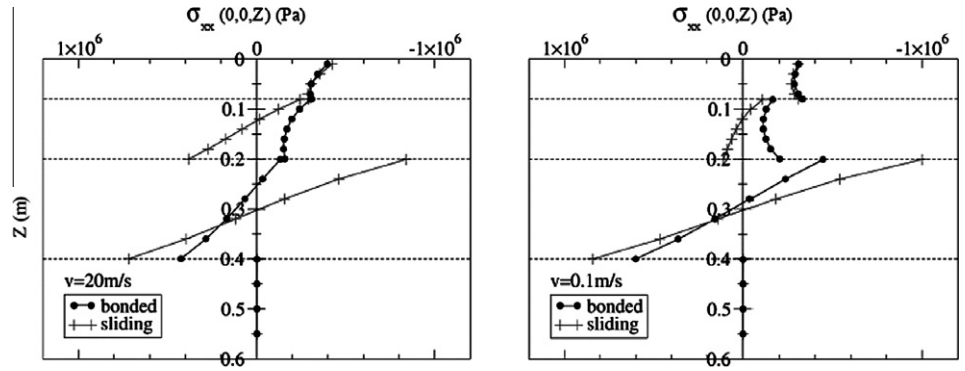

Fig. 8. Mechanical response under a moving load of a viscoelastic four-layer structure with a bonded or a slip boundary between layers 2 and 3: influence of the velocity on the normal stress (vertical profiles).

Fig. 8 shows the normal stress (σ_{xx}) as a function of depth for two velocities: $v = 20$ m/s and $v = 0.1$ m/s. The influence of the interlayer condition between layers 2 and 3 on the global response of the structure is also analyzed. For both bonded and sliding interface conditions, a decrease of the velocity goes along with an increase of the normal tensile and compressive stresses in layer 3 (material treated with hydraulic binders). The gain in normal stress is significant for the full bonded case but not for the sliding interface condition. Contrary to the trend observed in elastic layer 3, the normal stress decreases with velocity in asphalt layers. This is especially true for layer 2 when the sliding interface condition is considered. Besides, the normal stress within the subgrade (layer 4) is equal to zero. Indeed, because of high rigidity, the layer of materials treated with hydraulic binders forming the sub-base spreads and attenuates the stresses transmitted to the subgrade.

5. Conclusion

This article presented a semi-analytical method to compute the response of a layered viscoelastic medium under a uniform load moving at constant speed. Emphasis was put on the treatment of interlayer relations so that full bonded or sliding interface conditions could be considered (and mixed) in the solving process.

An algorithm based on the global matrix technique was used to compute the solution. Moreover, particular attention was paid to the treatment of singularities encountered when integrating the solution in the frequency domain to obtain the spatial response of the structure. The solution procedure was validated by comparison with engineering software ALIZE-LCPC which is used for the design of pavements in France.

The influence of the sliding interface condition on the response of a viscoelastic layered half-space was addressed through an application dedicated to pavement structures. The analysis was conducted on the longitudinal strain (ε_{xx}) and the normal stress (σ_{xx}).

The following concluding remarks are made: (i) deformations (extension and compression) are higher for the sliding interface condition than for the full bonded case. (ii) A discontinuity in ε_{xx} is observed at the location of the sliding interface; this discontinuity becomes larger as the load velocity decreases, i.e. as the behavior in viscoelastic layers gets more viscous. Moreover, at very low speeds, the maximum value of the longitudinal strain can be observed elsewhere than at the location of the sliding interface. (iii) The normal stress is also affected by the load velocity and the type of interface. The sliding interface condition leads to higher tensile stresses in the structure than does the full bonded case. Moreover, for interlayer slip, a decrease of the load speed goes along with a decrease of the normal stress in the viscoelastic layers and an increase of the normal stress in the elastic layer.

The method developed in this paper will allow, in future works, to easily introduce more complex contact laws between the layers of a structure.

Appendix A

A.1. $\mathbf{M}_i$ and $\mathbf{N}_i$ for the bonded condition

Substitution of Eqs. (18) and (20) in Eq. (22) leads to the determination of matrices $\mathbf{M}_i$ and $\mathbf{N}_i$. For the sake of making the layout look right, M_i is divided into submatrices:

$$\mathbf{M}_i = \begin{bmatrix} \mathbf{M}_i^- & \mathbf{M}_i^+ \end{bmatrix}, \tag{A.1}$$

where

$$\mathbf{M}_i^- = \begin{bmatrix} k_1 & 0 & \kappa_{si} \\ k_2 & \kappa_{si} & 0 \\ j\kappa_{pi} & jk_2 & jk_1 \\ -2\mu_i^* k_1 \kappa_{pi} & -\mu_i^* k_1 k_2 & -\mu_i^* \left(k_1^2 + \kappa_{si}^2\right) \\ -2\mu_i^* k_2 \kappa_{pi} & -\mu_i^* \left(k_2^2 + \kappa_{si}^2\right) & -\mu_i^* k_1 k_2 \\ -j\mu_i^* \left(k_1^2 + k_2^2 + \kappa_{si}^2\right) & -2j\mu_i^* k_2 \kappa_{si} & -2j\mu_i^* k_1 \kappa_{si} \end{bmatrix}, \tag{A.2}$$

$$\mathbf{M}_i^+ = \begin{bmatrix} k_1 & 0 & -\kappa_{si} \\ k_2 & -\kappa_{si} & 0 \\ -j\kappa_{pi} & jk_2 & jk_1 \\ 2\mu_i^* k_1 \kappa_{pi} & -\mu_i^* k_1 k_2 & -\mu_i^* \left(k_1^2 + \kappa_{si}^2\right) \\ 2\mu_i^* k_2 \kappa_{pi} & -\mu_i^* \left(k_2^2 + \kappa_{si}^2\right) & -\mu_i^* k_1 k_2 \\ -j\mu_i^* \left(k_1^2 + k_2^2 + \kappa_{si}^2\right) & 2j\mu_i^* k_2 \kappa_{si} & 2j\mu_i^* k_1 \kappa_{si} \end{bmatrix}. \tag{A.3}$$

$\mathbf{M}_i$ and $\mathbf{N}_i$ are the same for the continuity equation.

A.2. $\mathbf{M}_i$ and $\mathbf{N}_i$ for the sliding condition

The definition of $\mathbf{M}_i$ and $\mathbf{N}_i$ for sliding interfaces is obtained by inserting Eqs. (18) and (20) into Eq. (23) which is then expressed in a matrix form. $\mathbf{M}_i$ and $\mathbf{N}_i$ are split as follows:

$$\mathbf{M}_i = \begin{bmatrix} \mathbf{M}_i^- & \mathbf{M}_i^+ \end{bmatrix}, \quad \mathbf{N}_i = \begin{bmatrix} \mathbf{N}_i^- & \mathbf{N}_i^+ \end{bmatrix}, \tag{A.4}$$

where

$$\mathbf{M}_i^- = \begin{bmatrix} j\kappa_{pi} & jk_2 & jk_1 \\ -2\mu_i^* k_1 \kappa_{pi} & -\mu_i^* k_1 k_2 & -\mu_i^* \left(k_1^2 + \kappa_{si}^2\right) \\ -2\mu_i^* k_2 \kappa_{pi} & -\mu_i^* \left(k_2^2 + \kappa_{si}^2\right) & -\mu_i^* k_1 k_2 \\ 0 & 0 & 0 \\ 0 & 0 & 0 \\ j\mu_i^* \left(k_1^2 + k_2^2 + \kappa_{si}^2\right) & 2j\mu_i^* k_2 \kappa_{si} & 2j\mu_i^* k_1 \kappa_{si} \end{bmatrix}, \tag{A.5}$$

$$\mathbf{M}_i^+ = \begin{bmatrix} -j\kappa_{pi} & jk_2 & jk_1 \\ 2\mu_i^* k_1 \kappa_{pi} & -\mu_i^* k_1 k_2 & -\mu_i^* \left(k_1^2 + \kappa_{si}^2\right) \\ 2\mu_i^* k_2 \kappa_{pi} & -\mu_i^* \left(k_2^2 + \kappa_{si}^2\right) & -\mu_i^* k_1 k_2 \\ 0 & 0 & 0 \\ 0 & 0 & 0 \\ j\mu_i^* \left(k_1^2 + k_2^2 + \kappa_{si}^2\right) & -2j\mu_i^* k_2 \kappa_{si} & -2j\mu_i^* k_1 \kappa_{si} \end{bmatrix}, \tag{A.6}$$

$$\mathbf{N}_i^- = \begin{bmatrix} j\kappa_{pi} & jk_2 & jk_1 \\ 0 & 0 & 0 \\ 0 & 0 & 0 \\ -2\mu_i^* k_1 \kappa_{pi} & -\mu_i^* k_1 k_2 & -\mu_i^* \left(k_1^2 + \kappa_{si}^2\right) \\ -2\mu_i^* k_2 \kappa_{pi} & -\mu_i^* \left(k_2^2 + \kappa_{si}^2\right) & -\mu_i^* k_1 k_2 \\ -j\mu_i^* \left(k_1^2 + k_2^2 + \kappa_{si}^2\right) & -2j\mu_i^* k_2 \kappa_{si} & -2j\mu_i^* k_1 \kappa_{si} \end{bmatrix}, \tag{A.7}$$

$$\mathbf{N}_i^+ = \begin{bmatrix} -j\kappa_p & jk_2 & jk_1 \\ 0 & 0 & 0 \\ 0 & 0 & 0 \\ 2\mu_i^* k_1 \kappa_{pi} & -\mu_i^* k_1 k_2 & -\mu_i^* \left(k_1^2 + \kappa_{si}^2\right) \\ 2\mu_i^* k_2 \kappa_{pi} & -\mu_i^* \left(k_2^2 + \kappa_{si}^2\right) & -\mu_i^* k_1 k_2 \\ -j\mu_i^* \left(k_1^2 + k_2^2 + \kappa_{si}^2\right) & 2j\mu_i^* k_2 \kappa_{si} & 2j\mu_i^* k_1 \kappa_{si} \end{bmatrix}. \tag{A.8}$$

A.3. Definition of matrix $\boldsymbol{D}_0$

$\mathbf{D}_0$ is split into submatrices:

$$\mathbf{D}_0 = \begin{bmatrix} \mathbf{D}_0^- & \mathbf{D}_0^+ \end{bmatrix} \tag{A.9}$$

$\mathbf{D}_0^-$ and $\mathbf{D}_0^+$ act on $\boldsymbol{\beta}_1^-$ and $\boldsymbol{\beta}_1^+$, respectively. $\mathbf{D}_0$ expresses (20) in a matrix form and it is defined as follows:

$$\mathbf{D}_0^- = \begin{bmatrix} -2\mu_1^* k_1 \kappa_{p1} & -\mu_1^* k_1 k_2 & -\mu_1^* \left(k_1^2 + \kappa_{s1}^2\right) \\ -2\mu_1^* k_2 \kappa_{p1} & -\mu_1^* \left(k_2^2 + \kappa_{s1}^2\right) & -\mu_1^* k_1 k_2 \\ -j\mu_1^* \left(k_1^2 + k_2^2 + \kappa_{s1}^2\right) & -2\mu_1^* k_2 \kappa_{s1} & -2\mu_1^* k_1 \kappa_{s1} \end{bmatrix}, \tag{A.10}$$

$$\mathbf{D}_0^+ = \begin{bmatrix} 2\mu_1^* k_1 \kappa_{p1} & -\mu_1^* k_1 k_2 & -\mu_1^* \left(k_1^2 + \kappa_{s1}^2\right) \\ 2\mu_1^* k_2 \kappa_{p1} & -\mu_1^* \left(k_2^2 + \kappa_{s1}^2\right) & -\mu_1^* k_1 k_2 \\ -j\mu_1^* \left(k_1^2 + k_2^2 + \kappa_{s1}^2\right) & 2\mu_1^* k_2 \kappa_{s1} & 2\mu_1^* k_1 \kappa_{s1} \end{bmatrix}. \tag{A.11}$$

References

Andersen, L., Nielsen, S.R.K., 2003. Boundary element analysis of the steady-state response of an elastic half-space to a moving force on its surface. Engineering Analysis with Boundary Elements 27, 23–38.

Autret, P., Baucheron de Boissoudy, A., Marchand, J.P., 1982. ALIZE III practice. In: Proceedings of the 5th International Conference on Structural Design of Asphalt Pavements, Delft, Netherlands, 1982, pp. 174–191.

Barros, F.C.P., Luco, J.E., 1994. Response of a layered viscoelastic half-space to a moving point load. Wave Motion 19, 189–210.

Barros, F.C.P., Luco, J.E., 1995. Stresses and displacements in a layered half-space for a moving line load. Applied Mathematics and Computation 67, 103–134.

Burmister, D.M., 1943. The theory of stresses and displacements in layered systems and applications to the design of airport runways. In: Proceedings of the Highway Research Board 23, pp. 126–148.

Caron, J.F., Diaz Diaz, A., Carreira, R.P., Chabot, A., Ehrlacher, A., 2006. Multi-particle modelling for the prediction of delamination in multi-layered materials. Composites Sciences and Technology 66 (6), 755–765.

Chabot, A., Tran, Q.D., Ehrlacher, A., 2005. A simplified modeling for cracked pavements. Bulletin des Laboratoires des Ponts et Chaussées, pp. 258–259, 89–103. <http://www.lcpc.fr/en/sources/blpc/index.php>

Chabot, A., Chupin, O., Deloffre, L., Duhamel, D., 2010. Viscoroute 2.0: a tool for the simulation of moving load effects on asphalt pavement. RMPD Special Issue on Recent Advances in Numerical Simulation of Pavements 11(2), 227–250. (doi:10.3166/RMPD.11.227-250 © 2010 Lavoisier, Paris).

Chailleux, E., Ramond, G., Such, C., de la Roche, C., 2006. A mathematical-based master-curve construction method applied to complex modulus of bituminous materials. Roads Materials and Pavement Design 7 (EATA Special Issue), pp. 75–92.

Cole, J., Huth, J., 1958. Stresses produced in an half-space by moving loads. Journal of Applied Mechanics 25, 433–436.

Duhamel, D., Chabot, A., Tamagny, P., Harfouche, L., 2005. ViscoRoute: visco-elastic modeling for asphalt pavements. Bulletin des Laboratoires des Ponts et Chaussées, pp. 258–259, 89–103. <http://www.lcpc.fr/en/sources/blpc/index.php>.

Eason, G., 1965. The stresses produced in a semi-infinite solid by a moving surface force. International Journal of Engineering Sciences 2, 581–609.

Elseifi, M.A., Al-Qadi, I.L., Yoo, P.J., 2006. Viscoelastic modeling and field validation of flexible pavements. Journal of Engineering Mechanics (ASCE) 132 (2), 172–178.

SETRA-LCPC, 1997. French Design Manual For Pavement Structures, ed. SETRA-LCPC, Paris.

Frýba, L., 1972. Vibration of Solids and Structures under Moving Loads. Noordhoff, Groningen, The Netherlands.

Fryba, L., 1987. Dynamic interaction of vehicles with tracks and roads. Vehicle System Dynamics 16, 129–138.

Haskell, N.A., 1953. Dispersion of surface waves on multilayered media. Bulletin of the Seismological Society of America 43, 17–34.

Heck, J.V., Piau, J.M., Gramsammer, J.C., Kerzreho, J.P., Odeon, H., 1998. Thermo-visco-elastic modelling of pavements behaviour and comparison with experimental data from LCPC test track. In: Proceedings of the 5th BCRA, Trondheim, Norway.

Hopman, P.C., 1996. VEROAD: a viscoelastic multilayer computer program. Transportation Research Record 1539, 72–80.

Hornych, P., Kerzreho, J.P., Salasca, S., 2002. Prediction of the behaviour of a flexible pavement using finite element analysis with non-linear elastic and visco-elastic models. In: Proceedings of the ISAP 2002, Copenhagen.

Hornych, P., Chazallon, C., Allou, F., El Abd, A., 2007. Prediction of permanent deformations of unbound granular materials in low traffic pavements. Road Materials and Pavement Design 8 (4), 643–667.

Huet, C., 1963. Etude par une méthode d'impédance du comportement viscoélastique des matériaux hydrocarbonés. Université de Paris (France), Ph.D. thesis.

Huet, C., 1999. Coupled size and boundary-condition effects in viscoelastic heterogeneous and composite bodies. Mechanics of Materials 31, 787–829.

Hung, H.-H., Yang, Y.-B., 2000. Elastic waves in visco-elastic half-space generated by various vehicle loads. Soil Dynamics and Earthquake Engineering 21, 1–17.

Knopoff, L., 1964. A matrix method for elastic wave problems. Bulletin of the Seismological Society of America 54, 431–438.

Lowe, M.J.S., 1995. Matrix techniques for modeling ultrasonic waves in multilayered media. IEEE Transactions on Ultrasonics, Ferroelectrics, and Frequency Control 42 (4), 525–541.

Luco, J.E., Aspel, R.J., 1983a. On the Green's functions for a layered half-space: Part I. Bulletin of the Seismological Society of America 73, 909–929.

Luco, J.E., Aspel, R.J., 1983b. On the Green's functions for a layered half-space: Part II. Bulletin of the Seismological Society of America 73, 931–951.

Nilsson, R.N., Hopman, P.C., Isacsson, U., 2002. Influence of different rheological models on predicted pavement responses in flexible pavements. Road Materials and Pavement Design 3 (2), 117–147.

Nguyen, V.H., 2002. Comportement dynamique de structures non-linéaires soumises à des charges mobiles. ENPC (France), Ph.D. Thesis.

Olsson, M., 1991. On the fundamental moving load problem. Journal of Sound and Vibration 145 (2), 299–307.

Randall, M.J., 1967. Fast programs for layered half-space problems. Bulletin of the Seismological Society of America 57, 1299–1316.

Ricci, L., Nguyen, V.H., Sab, K., Duhamel, D., Schmitt, L., 2005. Dynamic behaviour of ballasted railway tracks: a discrete/continuous approach. Computers and Structures 83, 2282–2292.

Sayegh, G., 1965. Contribution à l'étude des propriétés viscoélastiques des bitumes purs et des bétons bitumineux. Faculté des Sciences de Paris (France), Ph.D. Thesis.

Schmidt, H., Jensen, F.B., 1985. Efficient numerical solution technique for wave propagation in horizontally stratified environments. Computers and Mathematics with Applications 11, 699–715.

Schmidt, H., Tango, G., 1986. Efficient global matrix approach to the computation of synthetic seismograms. Geophysical Journal of the Royal Astronomical Society 84, 331–359.

Schmidt, H., 1987. SAFARI: Seismo-acoustic fast field algorithm for range independent environments. User's Guide, SR 113, SACLANT ASW Research Centre, La Spezia, Italy.

Schmidt, H., 1999. OASES, Version 2.2, User Guide and Reference Manual,Department of Ocean Engineering Massachusetts Institute of Technology. <http://acoustics.mit.edu/faculty/henrik/oases/oases.html>.

Siddharthan, R.V., Yao, J., Sebaaly, P.E., 1998. Pavement strain from moving dynamic 3D load distribution. Journal of Transportation Engineering 124 (6), 557–566.

Siddharthan, R.V., Krishnamenon, N., Sebaaly, P.E., 2000. Finite-Layer approach to pavement response evaluation. Transportation Research Record 1709, 43–49.

Sneddon, I.N., 1952. The stress produced by a pulse of pressure moving along the surface of a semi-infinite solid. Rendiconti del Circolo Matematico di Palermo 2, 57–62.

Sun, L., 2006. Analytical dynamic displacement response of rigid pavements to moving concentrated and line loads. International Journal of Solids and Structures 43, 4370–4383.

Thomson, W.T., 1950. Transmission of elastic waves through a stratified solid medium. Journal of Applied Physics 21, 89–93.